Nuclear Materials and Energy 42 (2025) 101864

Contents lists available at ScienceDirect

Nuclear Materials and Energy

journal homepage: www.elsevier.com/locate/nme

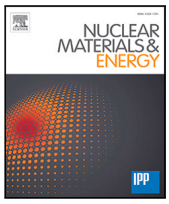

ERO2.0 predictions of nickel migration in the JET ITER-Like Wall

Pyry Virtanen [a,*], Henri Kumpulainen [a], Roni Mäenpää [a], Mathias Groth [a], Juri Romazanov [b], Sebastijan Brezinsek [b], JET contributors[1]

[a] Aalto University, Espoo, 02150, Finland
[b] Forschungszentrum Jülich GmbH, Institute for Energy and Climate Research Plasma Physics, Jülich, Germany

ARTICLE INFO

Keywords:
Nickel
Migration
ERO2.0
JET-ILW

ABSTRACT

Nickel transport in the Joint European Torus with the ITER-like wall (JET-ILW) is predicted using the 3D Monte-Carlo code ERO2.0, simulating the erosion and deposition of impurities in 3D geometry and utilizing hydrogenic background plasmas generated by the 2D edge fluid code EDGE2D-EIRENE. Charge exchange fluxes are obtained from the 3D neutral Monte-Carlo code EIRENE, which are modified to account for the shielding of the vacuum vessel wall by protruding plasma facing components, such as guard limiters. ERO2.0 is used to predict Ni erosion and deposition profiles for the first three JET-ILW campaigns weighted for the plasma operation time.

The primary location of nickel erosion on the Inconel vacuum vessel wall is predicted to be on the low-field side close to the midplane. The eroded nickel is predicted to be transported onto the entrance of the high-field side divertor, due to the scrape-off layer flows, where it is predicted to deposit and to form a layer on tile 1. The peak thickness of the predicted deposit layer is of the order $1\text{-}2\cdot10^{19}/cm^2$, a factor of six higher than measured in post-mortem tile analysis.

1. Introduction

Metallic plasma facing components (PFCs) in fusion devices are generally eroded by high-energy ions and atoms impacting the material surface and resulting in physical sputtering on the limiter and divertor surfaces. The Joint European Torus (JET) with the ITER-like wall (JET-ILW) contains PFCs in recessed areas, which are not plasma wetted, where the sputtering of the material is assumed to be dominated by charge exchange (CX) atoms. Previous studies have found significant quantities of nickel deposition on the high-field side (HFS) divertor [1]. In JET, the divertor is made of tungsten and the limiter surfaces are made of beryllium (Fig. 1). Beryllium has been found to deposit on the HFS divertor in JET in post-mortem analyses and WallDYN predictions [2] and in DIII-D tungsten is found to be transported to the HFS target [3]. According to measurements, the SOL flows primarily from the low-field side (LFS) midplane towards the HFS divertor [4] transporting the impurities to the HFS divertor.

Nickel is eroded from the recessed areas of the JET device, primarily, the vacuum vessel wall, which is made of Inconel, an alloy consisting primarily of nickel, chromium and iron [5]. In this publication, the migration of nickel in JET-ILW is simulated for the first three JET campaigns encompassing years 2011–2016 to elucidate the erosion and subsequent deposition of materials from recessed areas and the role CX atoms take in the migration process. The first three campaigns are chosen as extensive post-mortem analyses from the campaigns became available in 2019 [1].

In this paper, the erosion of the vacuum vessel wall through years 2011–2016 is simulated utilizing the ERO2.0 code to predict the primary location on the vacuum vessel wall from which nickel is eroded, the transport of the eroded nickel and the deposition of the nickel onto divertor surfaces, mainly the entrance of the HFS divertor.

2. Methodology

Nickel transport in the JET-ILW is simulated using ERO2.0, a Monte Carlo code, which predicts the erosion and deposition of impurities by simulating sputtering and impurity transport in a 3D geometry and on a given background plasma [6]. The required background plasma profiles, here 2D maps of the hydrogenic plasma and neutral conditions are obtained from EDGE2D-EIRENE, a code package which combines the edge plasma code EDGE2D [7] with the Monte Carlo kinetic neutral transport code EIRENE [8]. The EIRENE code simulates particle and heat transport in the scrape-off layer in 2D geometry. The COCONUT [9] package includes both EDGE2D-EIRENE and the

* Corresponding author.
E-mail address: pyry.l.virtanen@aalto.fi (P. Virtanen).
[1] See the author list of "Overview of T and D-T results in JET with ITER-like wall (Costanza F Maggi 2024 Nucl. Fusion)"

https://doi.org/10.1016/j.nme.2025.101864
Received 4 July 2024; Received in revised form 12 December 2024; Accepted 6 January 2025
Available online 13 January 2025

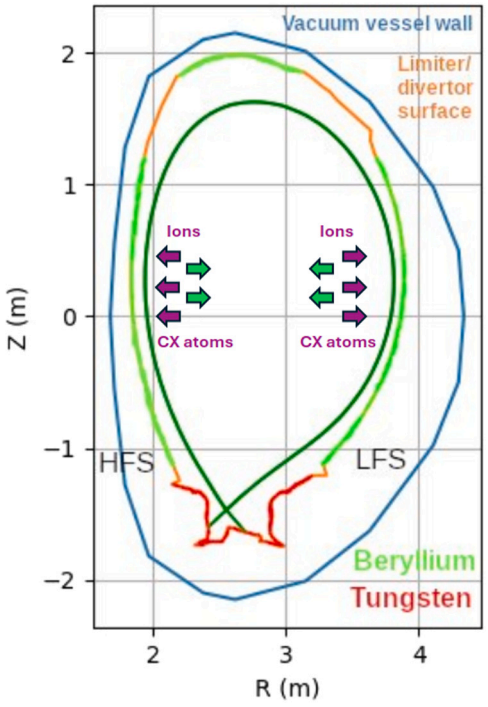

Fig. 1. Overview of the geometry of the JET vessel including the inconel vacuum vessel wall the limiter/divertor surface, beryllium marked with green, tungsten with red and open areas with orange. The separatrix of a VH configuration is included in dark green. The figure is derived from previous work [2]. (For interpretation of the references to colour in this figure legend, the reader is referred to the web version of this article.)

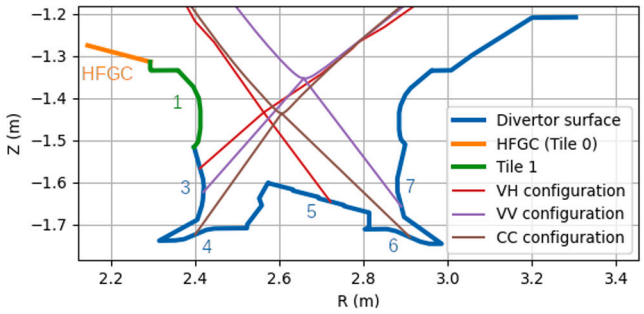

Fig. 2. Strike point locations in the divertor for VH (red), VV (purple) and CC (brown) configurations. HFGC (tile 0) is highlighted in orange and tile 1 in green, and the rest of divertor is shown in blue. (For interpretation of the references to colour in this figure legend, the reader is referred to the web version of this article.)

JETTO [10] fluid code for modelling 1D cross-field transport in the core plasma. As the focus of this project is not on core plasma modelling the impact of JETTO is minimal and EDGE2D-EIRENE is therefore the primary background plasma code. The background plasmas in this work are either existing scenarios or continued from the pre-existing scenarios. The 2D background plasma conditions are extrapolated onto the vacuum vessel wall using an exponential decay, with a decay length of 3 cm for electron and ion density and a decay length of 5 cm for electron and ion temperature. The 2D plasma profiles are axisymmetrically projected into 3D, whereas the 3D wall geometry is toroidally resolved in ERO2.0. The vacuum vessel wall is assumed to be pure nickel in the simulations. Radial transport is introduced by using an anomalous diffusion coefficient in the ERO2.0 simulations. The anomalous diffusion coefficient is set to 1 m^2/s. Drifts and any intrinsic impurities, such as Be and W, are omitted from the EDGE2D-EIRENE background plasmas, however ERO2.0 simulates $\vec{E} \times \vec{B}$ and $\nabla B \times \vec{B}$ drifts for nickel (and any other impurities the simulations include).

Post-processing the EDGE2D-EIRENE runs yields 2D profiles of the CX atomic fluxes into the divertor, low-field side (LFS) limiters, HFS limiters, and the top of the vacuum vessel (Z > 1.5 m). The CX atomic fluxes from EIRENE are energy resolved; in this work, the angular resolution of the CX atomic fluxes are omitted and a constant impact angle of 60° is used, which is close approximation of the effective impact angle for estimating sputtering of W in JET [11]. A single energy spectrum is used for the 2D CX atomic flux in the main chamber (Z > −1.2 m). The 2D profile is calculated to the edge of the computational grid used by EDGE2D-EIRENE, which extends up to the limiter and divertor surface (Fig. 1). The vacuum vessel wall in JET-ILW is a plasma facing component (PFC) which encapsulates all other PFCs. Since there are PFCs obstructing the CX atoms from reaching the vacuum vessel wall, the CX atomic flux predicted by EDGE2D-EIRENE is adjusted according to the fraction of the vacuum vessel wall being covered. The area directly below the divertor is 100% covered resulting in the CX atomic flux into this region being zero. At the LFS midplane approximately 40% of the vacuum vessel wall is screened by limiters and other protruding wall structures, resulting in a CX atomic flux of approximately 60% of the EDGE2D-EIRENE prediction. The top of the vacuum vessel (Z > 1.5 m) has varying levels of coverage of the vacuum vessel wall. At the LFS, the top coverage varies from 0% at the upper edge of the LFS limiters, increasing towards the maximum height of the vacuum vessel up to approximately 50%. At the HFS the coverage is approximately is 10% in the gap between the limiters and the ceiling limiters increasing to 60% and lowering to 50% at the maximum height of the vacuum vessel. Calculating the coverage at multiple Z locations for both the LFS and the HFS to creates a profile of the coverage.

The 2D coverage mask is applied to the 2D profile obtained from EDGE2D-EIRENE and the toroidally averaged 2D CX atomic flux profile to the vacuum vessel wall is determined. ERO2.0 assumes toroidal symmetry for the 2D CX atomic flux profile creating a 3D CX atomic flux profile. We note that not all PFCs in JET are accounted for in the simulations, such as the 'mushroom' limiters at the top of the vacuum vessel. The coverage percentages pertain to the PFCs, which are modelled in ERO2.0, including the LFS and HFS limiters, divertor tiles, HFS wall cladding tiles, antennas and upper beryllium limiters. The modelled surfaces account for most of the coverage especially around the midplane, but at the top of the vacuum vessel (Z > 1.5 m) the CX atomic flux to the vacuum vessel wall is higher as there are missing PFCs, due to missing 3D models for those PFCs.

There are four plasma configurations commonly used in JET, which are relevant for this project (Fig. 2). The four configurations include the vertical-horizontal (VH) configuration, for which one strikepoint is located on the HFS vertical part of the divertor (tile 3) and the second strike point is on the elevated part at the bottom of the divertor (tile 5), vertical-vertical (VV) configuration, for which the HFS strike point on the vertical tile 3 and the LFS strikepoint on the LFS vertical part of the divertor (tile 7), corner-corner configuration (CC), in which the strikepoints are at the bottom corners of the divertor (tile 4 on the HFS and tile 6 on the LFS) and the vertical-corner (VC) configuration, for which the strike points are on the HFS vertical (tile 3) and LFS divertor corner (tile 6). The HFGC (tile 0) and tile 1 form the HFS divertor top.

To predict the nickel erosion for the operational periods 20112016 in the JET-ILW, the predominant plasma operation scenarios for the configurations are identified. These scenarios (Table 1) utilize magnetic equilibria and EDGE2D-EIRENE grids of existing scenarios of specific JET pulses. For all scenarios with an input power of greater-than 5 MW an ELM version is created. However, the ELM scenarios are not included in the analyses conducted for this publication and are deferred to future publications, due to uncertainties in estimating the amount of time in the scenario being attributed to ELMs. Omitting the ELMs

Table 1
Plasma and divertor scenarios chosen to represent the first three JET-ILW campaigns. The input power is defined by the ELM-averaged net power entering the edge plasma, which is the sum of ohmic, neutral beam injection and radio frequency heating minus the observed core radiation. The first column is the configuration followed by the LFS midplane density, input power, total time for the scenario and the gross erosion rate for the scenario.

Configuration	LFS-midplane density (1e19 m^{-3})	P_{in} (MW)	Total time (s)	Gross nickel erosion rate (10^{20}/s)
VH	0.85	2.2	30 125	1.42
	1.8	2.2	12 965	0.19
	2.0	4.8	1880	0.82
	4.0	4.8	1668	0.29
	3.6	6.6	2397	1.39
	3.4	10	3716	2.57
	3.4	15	723	4.28
CC	0.85	2.2	34 112	5.82
	1.5	6	3877	3.73
	2.5	14	2426	7.25
	1.6	24	454	11.3
VC	0.85	2.2	28 096	0.85
	1.8	6	3263	0.85
VV	0.85	2.2	9971	6.39
	4.0	14	1764	6.39

results in decreased erosion. For the VH scenarios in Table 1: the first two are scenarios are L-mode plasmas at 2.5 MA/2.5 *T* with, continued from a pre-existing scenario based on JPN#81472 [12] at time 10 s. The following two VH scenarios are a set of ohmic-only heated plasmas at 2 MA/2 T, continued from a pre-existing scenario based on JPN#80295 [13] at 19 s, then one from a pre-existing scenario based on JPN#82486 [12] at 14 s with 2 MA/2 *T* and the last two are based on JPN#94605 [14] at 10 s with 2.3 MA/2.5 T. The background plasmas for the VH scenarios, with the exception of the 15 MW heating power scenario are directly taken from the above publications. The CC scenarios are continued from a pre-existing scenario based on JPN#96947 [14] at 8 s with 2.4 MA / 3.4 T, the VV scenarios are continued from a pre-existing scenario based on JPN#80821 [15] 21 s with 2 MA/2 T. Due to challenges in generating a suitable VC grid, the VC scenarios are simulated as CC scenarios, using JPN#96448 [16] at 10 s with 2.8 MA/2.5 *T* as the basis for the magnetic configuration. The LFS conditions are more important for the analysis in this paper, hence the CC configuration is the most analogous to the VC configuration as both have the LFS strike point in the divertor corner.

ERO2.0 is used to generate the erosion and deposition profiles for each individual scenario. The profiles are created by multiplying the deposition and erosion rate profiles from ERO2.0 by the total time for the scenario (Table 1). Adding the erosion and deposition profiles of each scenario together produces the net profile over the JET campaigns.

While in JET-ILW, the limiter phases are the most prevalent operational phases and increase erosion, they are omitted from the analysis due to challenges in modelling a limiter configuration background plasma and CX atomic flux profile. The importance of the limiter phases for the erosion and migration of nickel is deferred to a future publication.

3. Results and discussion

The modified CX atomic fluxes to the vacuum vessel wall are the highest on the LFS and are of the order of 10^{21} $m^{-2}s^{-1}$ (Fig. 3b). At the LFS midplane the CX atomic flux to the vacuum vessel wall is approximately 60% of the total atomic flux, as the limiters, antennae and other PFCs cover approximately 40% of the wall in this region.

The unmodified CX atomic flux (Fig. 3a) decreases towards the top on the LFS. Applying the wall coverage map to the vacuum vessel wall the CX atomic fluxes are more uniform, as the LFS top is much more open than the LFS midplane. These CX atomic fluxes to the LFS top are caused by a lower atomic density at the top than at the LFS midplane.

The poloidal distribution of the unmodified CX atomic flux to the limiter surfaces shows that on the HFS the gross CX atomic flux is predicted to be a factor of two to three lower than on the LFS (Fig. 3a). The lower CX atomic flux density is due to a lower atomic density. The modified CX atomic flux towards the HFS of the vacuum vessel wall is on the order of 10^{19} m^{-2}, approximately two orders of magnitude lower compared to the midplane on the LFS (Fig. 3b). The difference between the HFS and LFS modified CX atomic flux is in part due to high coverage of the HFS vacuum vessel wall by the limiters and other tiles leading to only approximately 5% of the total atomic flux going to the HFS vacuum vessel wall. While the comparison of the unmodified and the modified flux is only shown for the VH configuration with 10 MW of input power, the same procedure of CX atomic flux modification is used for all scenarios. Regardless of the scenario, the relative change from unmodified to modified flux is similar.

Nickel erosion decreases with an increase in density at the LFS midplane (Table 1), but increases with the input power for the VH cases. Additionally, the configuration of the plasma influences the erosion rate. The highest erosion rates are in the CC scenarios. For the VC scenarios, which are modelled as CC scenarios, erosion rates are approximately 20% of the lowest CC scenario are predicted. The difference in the gross erosion rate is due to a narrower plasma grid at the LFS in the CC scenario increasing the temperature at the edge of the EDGE2D grid compared to the VC scenario, resulting in higher extrapolated temperatures. In the VV scenarios the erosion rate did not change significantly between plasma conditions.

The primary location of gross nickel erosion at the vacuum vessel wall is predicted to be the low-field side (LFS) midplane, for which the CX atomic fluxes are at their largest (Fig. 4). The erosion zone continues up the vacuum vessel wall on the LFS. At the top of the vacuum vessel nickel erosion is predicted to occur at smaller quantities compared to the LFS midplane. The energy spectra from EDGE2D-EIRENE are applied to the entire main chamber, combining the energy spectra for the LFS midplane, the top and the HFS. Due to applying a single CX energy spectrum shared across all main chamber PFCs, the erosion is expected to be overpredicted at the top of the vacuum vessel, and underpredicted at the LFS, compared to the results expected with more spatially-resolved CX energy spectra. The CX atomic flux to the HFS wall is too low to cause significant erosion. ERO2.0 takes into account impurity self-sputtering and the sputtered nickel does itself erode nickel. The primary reason for the discrete spikes in the erosion profile is due to current limitations in the post-processing of the simulation output. The erosion profile from the vacuum vessel wall is projected back to the location of the limiter/divertor surface and the erosion is discretized to avoid double counting of eroded nickel. The spike in nickel erosion at S = 5.2 m corresponds with the upper edge of the LFS limiter, causing a protrusion in the geometry used for the S-coordinate. As the analysis of the erosion of vacuum vessel wall is qualitative, the profile still shows clearly that erosion is primarily occurring on the LFS near the midplane.

Nickel is sputtered as an atom and initially moves in a straight line. Most of the sputtered nickel is deposited back to the vacuum vessel wall due to the vessel geometry. For nickel atoms reaching the main SOL, they are ionized and follow the magnetic field lines and are entrained by the scrape-off layer (SOL) flows. In the simulated scenarios, the SOL flows from the LFS towards the top and subsequently down towards the HFS divertor entrance, going counterclockwise around the core plasma. Some scenarios, such as the low-density VH in L-mode confinement and the low-density CC H-mode confinement at moderate input power (Table 1), include significant flows towards the LFS divertor. In this publication, the EDGE2D-EIRENE predicted SOL flows are accepted without further modification. A more detailed description of the SOL flows in the various divertor plasma configurations and plasma scenarios is outside the scope of this publication. However, the uncertainties

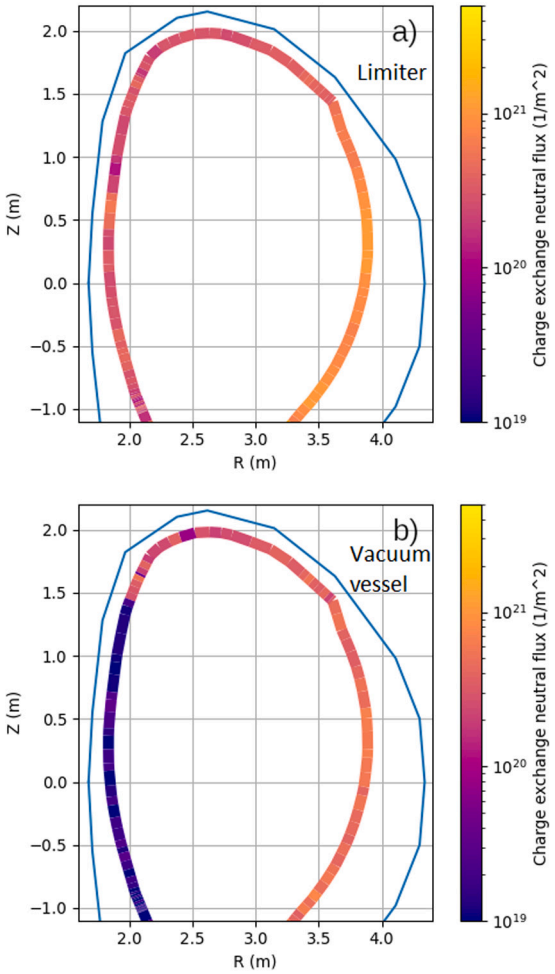

Fig. 3. Poloidal distribution of the CX atomic flux going to the limiters (a) and to the vacuum vessel wall (b). The distribution geometry follows the edge of the EDGE2D-EIRENE computation grid. The blue line represents the assumed projection of the modified CX fluxes mapped onto the vacuum vessel. The modified CX fluxes are identical for the limiter and vacuum surfaces. The case depicted in the figure is the VH 10 MW scenario. (For interpretation of the references to colour in this figure legend, the reader is referred to the web version of this article.)

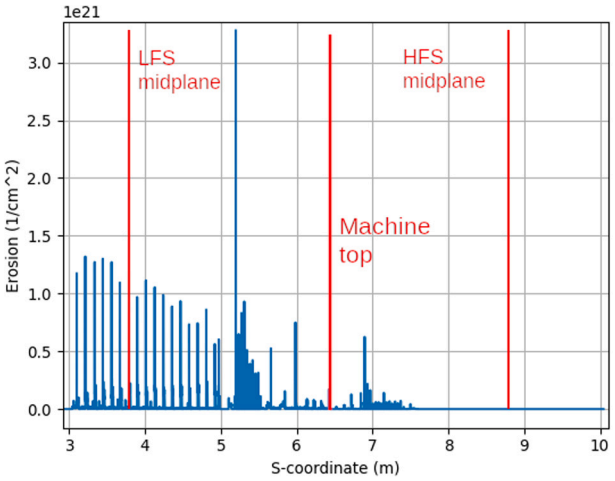

Fig. 4. ERO2.0 predicted poloidal distribution of gross nickel erosion on the surface of the vacuum vessel wall as a function of the S-coordinate, which is the distance along the divertor/limiter surface starting from the HFGC (S=0) and moving counterclockwise along the limiter/divertor surface. The plot does not show the divertor and starts at the LFS divertor entrance S=2.9 m and moves poloidally counterclockwise around the vessel towards the HFS.

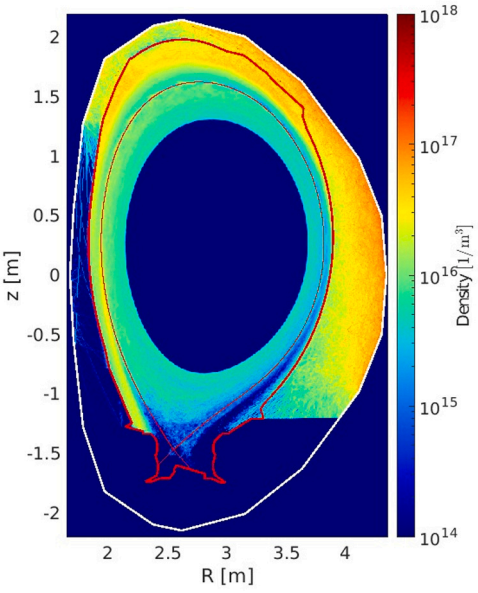

Fig. 5. Nickel density in the vacuum vessel as predicted by ERO2.0, outside of the divertor below z = −1.2 meters the vacuum vessel wall is inaccessible by atoms and ions, hence the particles are killed if they enter the region in the simulation.

associated with the predicted SOL flows is acknowledged and a detailed analyses deferred to a future publication. The SOL flows are predicted to transport the nickel onto the HFS and down towards tile 0, named the high field gap closure (HFGC), and the horizontal part of tile 1, where nickel is deposited.

Transport of nickel onto the HFS is observed in all plasma scenarios, comprising different combinations of input power, density and strike point configurations. The individual ERO2.0 scenario (Figs. 3 and 5)analysed is a VH scenario, with input power 10 MW and density of $3.4 \cdot 10^{19}$ m^{-3}, and uses the magnetic configuration of JPN#94605 at a time of 11 s. Transport into the LFS divertor is not observed in this particular scenario (Fig. 5).

The predicted gross nickel deposition onto tile 1 (Fig. 6) is at its thickest at the middle of the HFS divertor top (S ≈ 0.2 m), where the deposition is between $1\text{-}2{\cdot}10^{19}$ cm^{-2}. The re-erosion of nickel from tile 1 is not accounted for in the simulations, due to assuming that no pre-existing nickel deposits were on the tile. Due to simulating the ERO2.0 scenarios individually the homogeneous mixing model (HMM), which adjusts the composition of the tile dynamically, is also not utilized. However, the top of tile 1, which is of interest as post-mortem analysis of nickel deposition on the tile in the operational years 2011–2016 is available [1], is expected to experience re-erosion. However, a combination of factors restrict the re-erosion of nickel. Nickel has a relatively high energy threshold for erosion of approximately 50 eV, with peak yield around 150 eV [17]. The HFS divertor top is at the inner entrance of the HFS divertor and comprises of the horizontal part of tile 1 and the HFGC (Fig. 2). The HFS divertor top is located in a region of the SOL where the plasma temperature is not sufficient to cause significant sputtering of nickel. Sputtering is predicted to occur mostly due to CX atoms. The EDGE2D-predicted SOL flow is directly onto the top of the divertor, leading to prompt re-deposition of nickel ions onto the same location. Hence, inclusion of the re-erosion is expected not to lower the deposition on top of tile 1 significantly enough to affect the prediction of $1\text{-}2{\cdot}10^{19}$ cm^{-2} of gross nickel deposition.

Post mortem analysis of tile 1 show that for each of the three campaigns the net deposition is approximately 10^{18} cm^{-2} [1]. Assuming that re-erosion at the surfaces of these tiles is low, the deposition layer is on the order of $3{\cdot}10^{18}$ cm^{-2} at approximately S = 0.2 m. The top of

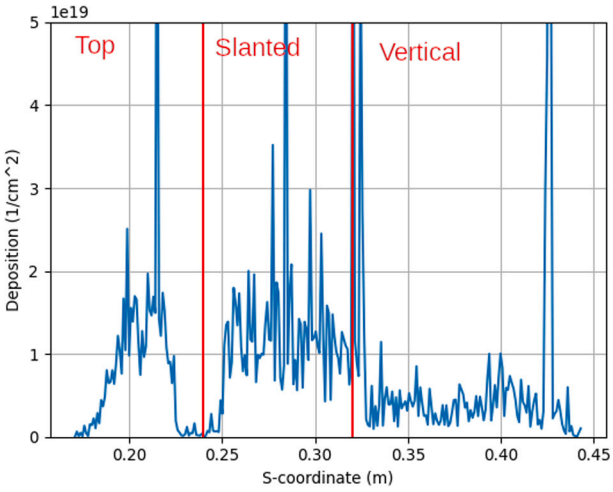

Fig. 6. ERO2.0 predicted bulk nickel deposition onto tile 1, after operation years 2011–2016 in JET as a function of the S-coordinate, which is the distance along the divertor/limiter surface starting from tile 0 and moving counterclockwise along the limiter/divertor surface, with markings of the expected deposition and re-erosion zones.

tile 1 is therefore predicted to be, within a factor of six of the post-mortem analysis results. On the other hand, the predicted deposition profile beyond the top of the tile does not reproduce the post-mortem analysis. Some of the difference is due to re-erosion as the HFS divertor shoulder across the slanted portion of tile 1 (Fig. 6), which experiences higher heat fluxes than the top leading to increased nickel re-erosion. Another hypothesis is that the transport in the scenarios selected is not spreading the nickel as evenly in the divertor as expected due to using a single magnetic equilibrium for the CC scenarios, a single magnetic equilibrium for the VC scenarios and a single magnetic equilibrium for the VV scenarios. For the VH scenarios four magnetic equilibria are used. Sharing the magnetic equilibria leads to some areas receiving increased or decreased deposition compared to having more equilibrium profiles. The HFGC (tile 0) in the current simulations does not show significant nickel deposition despite the high densities of nickel above the tile (Fig. 5), which is inconsistent with post mortem-analysis. The root cause of the discrepancy is currently unknown.

4. Conclusions

ERO2.0 simulations executed on hydrogenic EDGE2D-EIRENE background plasma predict that the main erosion location of nickel from the vacuum vessel wall is the LFS vacuum vessel wall, close to the midplane, due to the CX atomic fluxes being predicted strongest in this region. The CX atomic fluxes to the vacuum vessel wall are significant on the LFS because of the large gaps between the limiters and antennas, and the atomic densities being at their highest in the main chamber. On the HFS the Be limiters and the recessed, Be coated tiles block 95% of the flux towards the vacuum vessel wall. The top of the vacuum vessel is not covered with Be coated tiles, however the CX atomic fluxes are lower than to the LFS midplane, due to lower predicted atomic densities. A part of the sputtered nickel is transported from the vacuum vessel wall into the main SOL where nickel ions are entrained in the predicted SOL flows and be transported towards the HFS divertor top, where they are deposited, forming a co-deposit layer containing nickel. The highest areal density of the nickel deposit layer is predicted on tile 1, of the order of $1\text{-}2\cdot10^{19}$ cm^{-2}, within a factor of six of what is observed in post mortem analyses. The differences between post-mortem analyses of tiles and the predicted deposition layer are likely due to omitting re-erosion and the limited number of magnetic equilibria used for the combined profile. Additionally, impurity transport in the SOL is determined by the SOL flows and the uncertainty in the SOL flow introduces uncertainty to the deposition profiles.

The net erosion profile of nickel from the vacuum vessel wall requires calculating the deposition profile of nickel on the vacuum vessel wall, which is currently not possible in post-processing of the ERO2.0 simulations. On the HFGC (tile 0) there is insignificant nickel deposition, which is inconsistent with post-mortem analyses. The exact role of the limiter phase for nickel erosion has to be confirmed and ELMs are currently not included in the modelling of the deposition.

CRediT authorship contribution statement

Pyry Virtanen: Writing – review & editing, Writing – original draft, Methodology, Conceptualization. **Henri Kumpulainen:** Methodology, Conceptualization. **Roni Mäenpää:** Methodology. **Mathias Groth:** Writing – review & editing, Supervision. **Juri Romazanov:** Software. **Sebastijan Brezinsek:** Writing – review & editing, Supervision.

Declaration of competing interest

The authors declare that they have no known competing financial interests or personal relationships that could have appeared to influence the work reported in this paper.

Acknowledgements

This work has been carried out within the framework of the EUROfusion Consortium, funded by the European Union via the Euratom Research and Training Programme (Grant Agreement No 101052200 — EUROfusion). Views and opinions expressed are however those of the author(s) only and do not necessarily reflect those of the European Union or the European Commission. Neither the European Union nor the European Commission can be held responsible for them. The calculations presented above were performed using computer resources within the Aalto University School of Science “Science-IT” project.

Data availability

The authors do not have permission to share data.

References

[1] A. Widdowson, et al., Deposition of impurity metals during campaigns with the JET ITER-like Wall, Nucl. Mater. Energy 19 (2019) 218.
[2] S. Brezinsek, et al., Beryllium migration in JET ITER-like wall plasmas, Nucl. Fusion 55 (6) (2015) 063021.
[3] J.D. Elder, P.C. Stangeby, E.A. Unterberg, T. Abrams, J.A. Boedo, D. Donovan, A.G. McLean, D.L. Rudakov, W.R. Wampler, J.G. Watkins, Evidence of near-SOL tungsten accumulation using a far-SOL collector probe array and OEDGE modelling in the DIII-D metal rings L-mode discharges, Nucl. Mater. Energy 19 (2019) 287–294.
[4] Nobuyuki Asakura, Understanding the SOL flow in L-mode plasma on divertor tokamaks, and its influence on the plasma transport, J. Nucl. Mater. 363–365 (2007) 41–51, Plasma-Surface Interactions-17.
[5] Special Metals Corporation, Inconel alloy 600, 2008, Accessed 11 November 2024.
[6] J. Romazanov, D. Borodin, A. Kirschner, S. Brezinsek, S. Silburn, A. Huber, V. Huber, H. Bufferand, M. Firdaouss, D. Brömmel, et al., First ERO2.0 modeling of Be erosion and non-local transport in JET ITER-like wall, Phys. Scr. 2017 (T170) (2017) 014018.
[7] R. Simonini, G. Corrigan, G. Radford, J. Spence, A. Taroni, Models and numerics in the multi-fluid 2-D edge plasma code EDGE2D/U, in: Contributions to Plasma Physics, 34, (2–3) Wiley Online Library, 1994, p. 368.
[8] S. Wiesen, et al., EDGE2D/EIRENE Code Interface Report, JET ITC-Report 8, 2006.
[9] M. Fichtmüller, et al., Core-edge coupling and the effect of the EDGE on overall plasma performance, Czech. J. Phys. 48 (2) (1998) 25.
[10] G. Cenacchi, A. Taroni, JETTO a Free Boundary Plasma Transport Code, Technical report, ENEA, 1988.
[11] H. Kumpulainen, et al., Impact of co-dependent energy and angular atomic impact spectra on tungsten erosion in JET, in: The 21st International Congress on Plasma Physics, 2024.

[12] H.A. Kumpulainen, et al., Validation of EDGE2D-EIRENE and DIVIMP for w SOL transport in JET, Nucl. Mater. Energy 25 (2020) 100866.
[13] H.A. Kumpulainen, M. Groth, M. Fontell, A.E. Jaervinen, G. Corrigan, D. Harting, Comparison of DIVIMP and EDGE2D-EIRENE tungsten transport predictions in JET edge plasmas, Nucl. Mater. Energy 25 (2020) 100784.
[14] H.A. Kumpulainen, et al., ELM and inter-ELM tungsten erosion sources in high-power, JET ITER-like wall H-mode plasmas, Nucl. Mater. Energy 33 (2022) 101264.
[15] V. Solokha, et al., The role of drifts on the isotope effect on divertor plasma detachment in JET ohmic discharges, Nucl. Mater. Energy 25 (2020) 100836.
[16] L. Horvath, et al., Pedestal particle balance studies in JET-ILW H-mode plasmas, Plasma Phys. Control. Fusion 65 (4) (2023) 044003.
[17] W. Eckstein, Sputtering yields, Vacuum 82 (9) (2008) 930–934, Selected Papers from the 18th Ion Surface Interactions Conference, Zvenigorod, Russia, 24-28 2007.